Molecular Differences between Hydrocarbon and Fluorocarbon Surfactants at the CO_2/Water Interface

Matthew T. Stone,[†,‡,§] Sandro R. P. da Rocha,[||] Peter J. Rossky,*[,†,‡,§] and Keith P. Johnston[†,§]

Department of Chemical Engineering, Institute for Theoretical Chemistry, and Department of Chemistry and Biochemistry, University of Texas at Austin, Austin, Texas 78712, NSF-STC—Environmentally Responsible Solvents and Processes, The University of North Carolina at Chapel Hill, Chapel Hill, North Carolina 27599, and Department of Chemical Engineering and Materials Science, Wayne State University, Detroit, Michigan 48202

Received: May 22, 2003

Fundamental molecular understanding of surfactants at the CO_2/water interface is lacking, especially in the context of the poor performance of hydrocarbon-based surfactants relative to fluorocarbons. We present computer simulations of a dichain fluorinated phosphate surfactant known to promote microemulsion formation and its hydrocarbon analogue which does not. Analysis of the computer simulation results shows that CO_2 solvates both tails well. In fact, at equal area per surfactant, CO_2 penetrates the hydrocarbon tails somewhat more than the fluorocarbon tails. Water is also found to penetrate the hydrocarbon surfactants to a greater extent than the fluorocarbon ones. This difference in penetration causes an unanticipated orientation of the headgroup in the fluorocarbons that promotes hydration and is absent in the hydrocarbon surfactant case. These results, combined with the structural analysis, lead us to infer that the poor performance of hydrocarbon surfactants is caused by their inability to effectively separate the water and CO_2 phases from each other. A geometrically based penetration parameter for surfactants is defined and calculated. This parameter describes the ability of the surfactants to physically separate the bulk phases. The parameter is shown to correlate with interfacial tension. On the basis of this mechanism for surfactant performance, "stubby" hydrocarbon surfactants, which cover more surface area per surfactant, show promise for new surfactant design.

1. Introduction

The formation of water in CO_2 microemulsions offers a new approach to biological processes,[1,2] organic synthesis,[3] nanoparticle chemistry,[4] and dry cleaning.[5] CO_2/water dispersions have many advantages over conventional solvents. CO_2 is a nontoxic, environmentally friendly substitute for traditional organic solvents. Also, CO_2 has advantageous physiochemical and transport properties that might make it a superior choice. Formation of microemulsions requires the use of an excellent surfactant for the CO_2/water interface.[1]

Several issues regarding the use of CO_2 in these processes need to be addressed. The surfactant must be relatively inexpensive to produce and form microemulsions at reasonable pressures, typically below 35 MPa. Fluorocarbon surfactants, which form microemulsions at reasonable pressures, can be costly and environmentally unfriendly. Even so, only a few fluorinated surfactants, for example, PFPE (perfluoropolyether),[1,6,7] fluorinated AOT (aerosol-OT, sodium bis(2-ethylhexyl)sulfosuccinate) analogues,[8−15] and fluorinated phosphates,[16,17] can form microemulsions. Hydrocarbon surfactants are currently unsuitable for many applications because of their inability to stabilize microemulsions at reasonable pressures. Nevertheless, hydrocarbons are less expensive and less harmful to the environment. Experimental efforts to this point have been largely unsuccessful in finding suitable hydrocarbon-based surfactants,[8] although a few researchers have achieved some water uptake into CO_2 using branched hydrocarbon surfactants.[18−20] Currently, there is little fundamental understanding of the reasons that fluorocarbons are far superior surfactants than hydrocarbons.

Despite the technological interest, the science behind surfactant function in CO_2 is not well understood. Initially, since so few nonvolatile compounds dissolve in CO_2 to any appreciable extent, the approach to making better surfactants focused on finding tails that are more CO_2-philic.[8,21] Later, the need for a balance between hydrophilic and CO_2-philic forces in the surfactant became well recognized.[22] Not only is a tail that dissolves in CO_2 desirable, but the proper balance is needed to make excellent surfactants. The present work approaches the basis for surfactant quality from a molecular viewpoint by looking at two surfactants, DiF8 and its hydrocarbon analogue, using computer simulation. DiF8 is an excellent surfactant in CO_2/water systems,[16] whereas efforts to use hydrocarbon analogues of DiF8 have been unsuccessful.

Formation of a microemulsion requires a surfactant with some specific properties. First, the surfactant must be interfacially active.[15,23] This can be achieved by varying the chemical makeup of both the headgroup and the tail.

Second, the surfactant must be able to lower the interfacial tension to nearly zero.[15,23] This is achieved through the replacement of the CO_2/water interface with a water/head and a CO_2/tail interface, with each of these new interfaces having an interfacial tension near zero.

Finally, the surfactant must be compatible with the curvature of the microemulsion droplets.[23] In the case of water in CO_2 microemulsions, this requires that the repulsion between hy-

* Corresponding author.
† Department of Chemical Engineering, University of Texas at Austin.
‡ Institute for Theoretical Chemistry and Department of Chemistry and Biochemistry, University of Texas at Austin.
§ NSF-STC—Environmentally Responsible Solvents and Processes.
|| Wayne State University.

10.1021/jp035422k CCC: $25.00
Published on Web 08/26/2003

DiF8

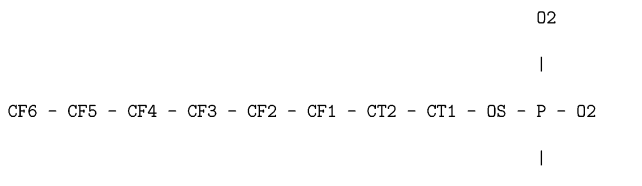

DiH8

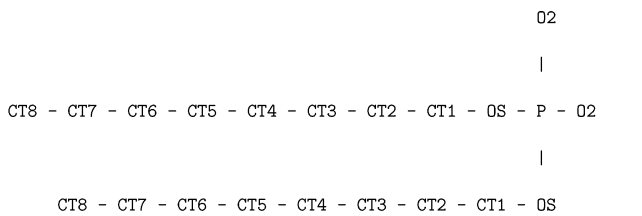

Figure 1. Nomenclature scheme and structure for DiF8 and DiH8. All explicit fluorines, hydrogens, and sodium ions are omitted for clarity. Attached to every CT carbon are hydrogens. All CF carbons have fluorine attached. The OPLS parameters[35] used can be found in Table 1S.

drophilic headgroups be weaker than the tail−tail repulsion. The surfactant then preferentially curves around the water phase, resulting in a water in CO_2 microemulsion. Here, we focus on understanding the lowering of interfacial tension between CO_2 and water by hydrocarbon and fluorocarbon surfactants. This is an important issue and may be the distinguishing characteristic between hydrocarbon and fluorocarbon surfactants.

Few detailed simulations of the CO_2/water interface have been performed. da Rocha et al. have characterized the neat CO_2/water interface.[24] They have also looked at a CO_2/water interface with PFPE surfactant.[25] Wipff and co-workers have focused on the behavior of ions at the interface and its applications to liquid−liquid extraction.[26−28] Salaniwal et al. have performed simulations of aggregate formation in carbon dioxide using a united atom model of the surfactant.[29,30] Senapati et al. have characterized a model fluorocarbon surfactant micelle using both simulation and small angle neutron scattering (SANS) experiments.[31] Hence, there is considerable opportunity to learn about related systems though simulation.

This paper is organized as follows. In section 2, we discuss the methodology. Section 3 describes our thermodynamic and structural results for the two surfactants. In section 4, we present our conclusions.

2. Methodology

2.1. Molecules Studied. In this study, we have looked at two surfactants, one of which has been shown to be a good surfactant for CO_2/water systems, and the other is the hydrogenated analogue of this surfactant. The good surfactant we have studied is termed DiF8. It is a double tail phosphate surfactant with a fluorinated tail, $Na^+ {}^-O_2P(OCH_2CH_2(CF_2)_5CF_3)_2$. The other molecule, DiH8, is chemically similar to DiF8 except that DiH8 has no fluorine. Its chemical formula is $Na^+ {}^-O_2P(O(CH_2)_7CH_3)_2$. Figure 1 describes a labeling scheme for both surfactants.

2.2. Models. For CO_2, we have used the EPM2 model with fixed bond angles and lengths described by Harris and Yung.[32] Water is modeled using the SPC/E water model.[33] Both of these models have been shown to reproduce the phase behavior of each compound accurately. Since *PVT* effects might be important, especially near the critical point of CO_2, accurately reproducing the equation of state of these components is important. The simulated surface tension of the neat CO_2/water interface (∼33 mN/m)[24] with the same model is approximately 50% larger than the one experimentally determined value (∼20 mN/m).[22] Other experimental estimates suggest the surface tension may be higher, reducing the discrepancy.[34] To model the surfactant, we have used the OPLS potential model developed by Jorgensen.[35] Cross parameters for Lennard-Jones interactions are calculated using the Lorentz−Berthelot mixing rules. All the parameters for the force field are provided in the Supporting Information (Table 1S).

We use the DL_POLY molecular simulation package to perform the molecular dynamics simulations.[36] The system contains 324 carbon dioxide molecules and 793 water molecules. The water and CO_2 regions are separated by two planar interfaces under periodic boundary conditions. Each interface contains eight surfactant molecules, except for the simulation of DiH8 at the smallest area per surfactant, where there are 12 surfactants.

We have modified DL_POLY to perform simulations in two different ensembles. The modified code solves the dynamics equations for constant normal pressure and either constant area per surfactant or zero surface tension. The new equations are described in the sections detailing the algorithms below. Equilibration required 500 ps for constant area simulations, while the zero interfacial tension ensemble required 1 ns. The simulation parameters, such as the time step and the Ewald summation tolerance, can be found in Supporting Information Figure 1S, which is a sample input file to DL_POLY.

2.3. Constant Normal Pressure Algorithm. Experimentally, the pressure on an emulsion drop is oriented normal to the interface. Due to the interfacial tension, the pressure tangential to the interface is lower than the normal pressure. Traditional constant pressure molecular dynamics algorithms are isotropic and vary all cell vectors in an attempt to fix the average of the tangential and normal pressures. With an interface, this results in a normal pressure that differs from the target pressure. To address this issue, we follow ref 38 and impose a constant normal pressure ensemble. In a constant normal pressure ensemble, a pressure is imposed in one direction in the MD cell (the *z*-direction), and in the other orthogonal directions, the lengths of the cell are fixed. To impose this ensemble, we have employed the methodology of Parrinello and Rahman.[37] Zhang et al. have employed a similar methodology and use slightly different notation.[38] The extended Lagrangian for systems for N particles with external stresses is[37]

$$L = {}^1/_2\sum_{i=1}^{N} m_i v_i^2 - \sum_{i=1}^{N}\sum_{j>i}^{N} \phi_{ij}(r_{ij}) + {}^1/_2 MTr(\dot{h}'\dot{h}) - pV \quad (1)$$

where h is a matrix containing the vectors describing the MD cell boundaries, p is the imposed pressure, M is an arbitrary mass, ϕ is the interaction potential between particles, m and v are the particle mass and velocity, and V is the system volume.

We impose constraints upon this system. Choosing direction 3 as the *z*-direction, which is normal to the interface, these constraints are expressed as

$$\dot{h}_{i,i}(t) = 0 \qquad \text{for all } t \text{ and } i = 1, 2 \tag{2}$$

$$h_{i,j}(t) = 0 \qquad \text{for all } t \text{ and } i \neq j \tag{3}$$

Directions 1 and 2 are the *x*- and *y*-axes, which are symmetric. Essentially, these constraints constrain the *x* and *y* cell lengths to be fixed in time, and all cell vectors are constrained to be at right angles. The *z*-direction is allowed to fluctuate.

Parrinello and Rahman have derived the equations of motion from this Lagrangian, and the extension including the above constraints is simple. The equation of motion for the cell vector is

$$M\ddot{h}_{3,3} = (\Pi_{3,3} - p)h_{1,1}h_{2,2} \tag{4}$$

Π is the pressure tensor.

2.4. Zero Interfacial Tension Ensemble. Forming microemulsions requires an extremely low value of the interfacial tension. To simulate systems at extremely low interfacial tension, we have decided to impose a condition of zero interfacial tension for some of the simulations performed. The ensemble we have employed is listed explicitly by Zhang et al.,[38] and we only summarize the results here.

The equations of motion for the cell sides in the ensemble of $Np_n\gamma T$ are

$$M\ddot{h}_{1,1} = h_{1,1}(\gamma_s - \gamma_m) \tag{5}$$

$$M\ddot{h}_{3,3} = h_{1,1}{}^2(\Pi_{3,3} - p_n) \tag{6}$$

and

$$\gamma_m = h_{3,3}(p_n - 0.5(\Pi_{1,1} + \Pi_{2,2})) \tag{7}$$

where p_n is the set normal pressure and γ_s is the set interfacial tension. These equations also reflect the imposition of a square shape to the interface; that is, $h_{1,1}$ is constrained to be equal to $h_{2,2}$. In the case of zero interfacial tension, the equation of motion for the tangential sides of the box reduces to

$$M\ddot{h}_{1,1} = h_{1,1}h_{3,3}(0.5(\Pi_{1,1} + \Pi_{2,2}) - p_n) \tag{8}$$

3. Results

We have performed five simulations under different conditions as described in Table 1. The surface tensions are calculated using the pressure differential formula,

$$\Gamma = 0.5(\Pi_{3,3} - 0.5(\Pi_{1,1} + \Pi_{2,2}))l_z \tag{9}$$

l_z is the length of the simulation box in the *z*-direction. The leading factor of 0.5 merely accounts for the presence of two interfaces in our simulation.

We consider the simulation of DiF8 at the smallest area first. 58 Å^2 per molecule was initially chosen as the area because it can be inferred from data from Steytler et al.[17] A similar area is calculated by Senapati et al. from SANS data.[31] Yet, 58 Å^2 is quite a small area compared to available data for other CO_2/water surfactants. For PFPE, the area is between 76 and 107 Å^2 depending on temperature.[39] The equilibration period alone was sufficient to establish that the apparent interfacial tension from simulation at 58 Å^2 would be negative, indicating that this area is too small for the molecular model used. To address this problem, we performed a simulation at zero surface tension (simulation F90). Simulation F90 shows that the area in this case is ~90 Å^2 per surfactant, which is comparable to that for PFPE. A fixed area simulation at 116 Å^2 (F116) is consistent, with a surface tension of about 15 mN/m.

TABLE 1: Overview of Simulations Performed[a]

simulation label	surfactant	ensemble[b]	area per surfactant (Å^2)	surface tension (mN/m)	production run length (ns)
F116	DiF8	CNP	116	14.9 ± 1.4	1.5
F58[c]	DiF8	CNP	58	-22 ± 5	
F90	DiF8	ZST	90.5 ± 0.7	-0.5 ± 2	1.0
H116	DiH8	CNP	116	22.5 ± 1.5	1.0
H80	DiH8	CNP	80	4.3 ± 1.5	1.0

[a] All simulations are performed at 318 K and 20 MPa normal pressure. Simulations are labeled by a symbol for later reference. [b] CNP denotes a constant normal pressure ensemble, whereas ZST denotes a zero surface tension ensemble. [c] The averages reported are over the equilibration period of 500 ps; no production run has been performed.

Comparing the two surfactants, the simulations at constant normal pressure and comparable areas show that the surface tension is systematically higher for the hydrocarbons (see Table 1). Comparing these surfactants at similar area per headgroup is reasonable because one might expect the areas of these two surfactants to be similar. The area per headgroup is primarily affected by the interfacial tension in the absence of surfactant and the activity of the surfactant at the interface. For DiF8 and DiH8, the first of these factors is identical. The activity of the surfactants is different, but on the basis of CO_2/water balance arguments,[22] one might expect DiH8 to be less interfacially active, as the balance would favor water more strongly, compared to DiF8. Reduced surface activity would cause a larger area per headgroup for DiH8, which would make it an even less effective surfactant than indicated by an equal area comparison; the interfacial tension increases as the area per headgroup increases, as can be shown by simple models.[39]

We next consider structural features corresponding to these thermodynamic observations. We consider first tail chain extension, which one would correlate with the effectiveness of tail solvation. We use the density distribution of the carbon atoms in the tail to report tail extension. The density of the carbon atoms is measured relative to the average *z*-plane of the phosphorus atoms, $z = z_p$, which is given by

$$z_p = \frac{1}{N}\sum_1^N z(P_i) \tag{10}$$

where N is the number of atoms in that particular interface and $z(P_i)$ is the z component of the position vector for phosphorus atom P_i. All results below report an average of both interfaces present in our simulation.

Figure 2 shows the extension of the tails away from the average phosphorus plane. All of the systems show nearly identical extension into the CO_2 phase. The difference in peak heights is not significant, being primarily caused by the different surface densities at each condition. On the basis of this measure, hydrocarbon and fluorocarbon tails appear to be adequately and comparably solvated by CO_2. Further evidence of effective solvent penetration of the hydrocarbon tails by CO_2 is found in the CO_2 density profiles relative to the average phosphorus plane, shown in Figure 3. CO_2 mixes into the tail region at least as much for hydrocarbon as for fluorocarbon surfactants. In fact, at 116 Å^2 (simulations F116 and H116), CO_2 evidently penetrates the hydrocarbon tails to a greater extent than the fluorocarbon tails. This point will be discussed more extensively later. Salinwal et al. claim a slight shift in the tail density for a hydrocarbon surfactant using different models for the tail

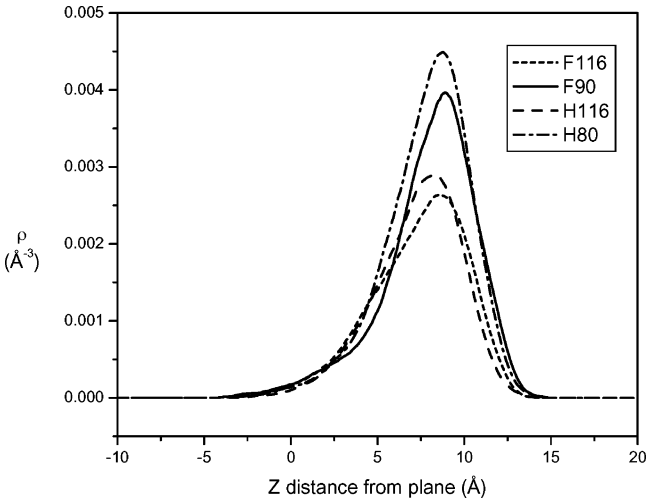

Figure 2. Density of terminal carbon atoms from the average *z*-plane of the phosphorus atoms. The difference in peak heights results primarily from concentration differences.

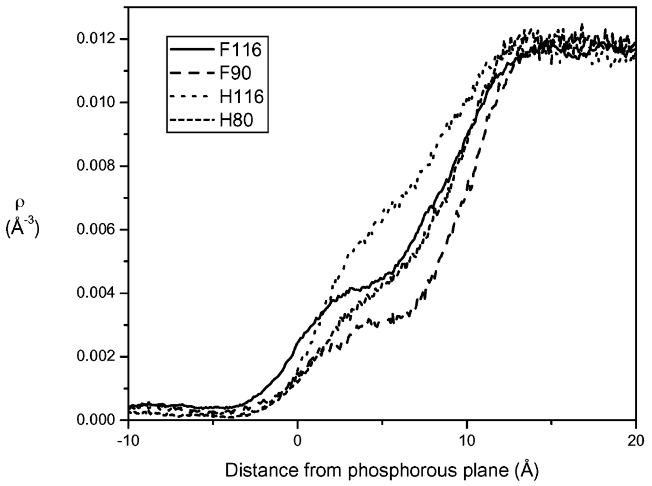

Figure 3. Density of carbon atoms in CO_2 measured from the average phosphorus plane, for fluorocarbon and hydrocarbon surfactants.

groups.[29] Despite the ongoing work to search for more CO_2-philic tails,[8,21] these results suggest that differences in the solvation of the tails are not the key to explain the differences between these surfactants.

Despite their structural similarities, hydrocarbon and fluorocarbon surfactants are also found to differ in the interaction of water with the headgroup. Figure 4 shows the coordination number of the phosphate ether oxygen (OS) atoms in each simulation. A water molecule is defined to coordinate an OS atom if it lies within 3.5 Å of that OS atom. The figure shows that the fluorocarbons have distinctly more OS atoms with zero water coordinating them than do the hydrocarbons. The pair correlation function between the water oxygen and the second carbon from the phosphorus atom (CT2), as seen in Figure 5, shows additional water density near the CT2 carbon for the hydrocarbons relative to the fluorocarbons. The CT2 carbon is chosen for comparison because it is the same number of carbons away from the headgroup and is the same size for both surfactants. Comparing carbons further down the chain, where the carbon is fluorinated in DiF8, would complicate the analysis. Much of the difference in these correlation functions can be attributed to fluorine being larger than hydrogen. The drop in water density at the CT2 carbon suggests that the fluorocarbon surfactant "repels" water better than the hydrocarbon surfactant. Experiments also support this view. Murkerjee and Handa show

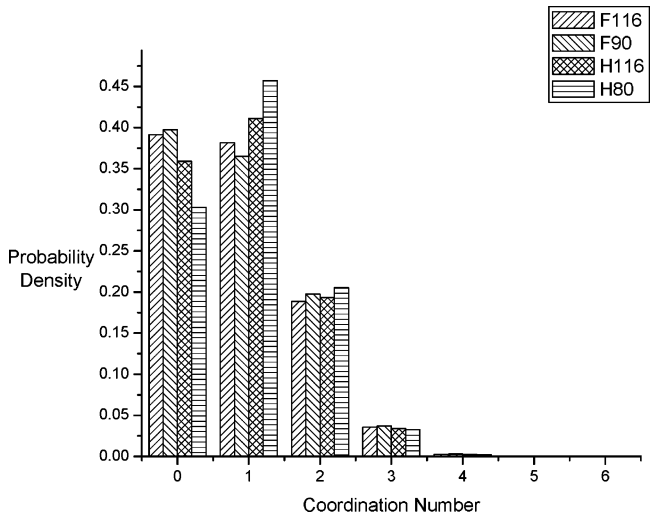

Figure 4. Coordination number of water from the OS atoms. The plot shows the probability of finding a particular OS atom with *n* water molecules coordinating it.

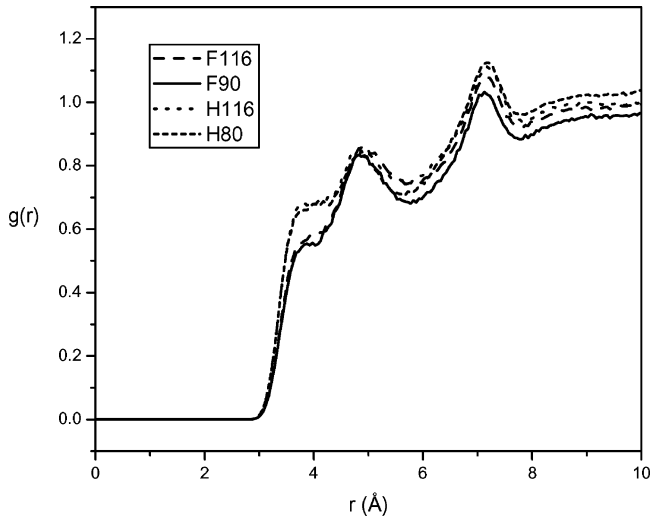

Figure 5. Pair correlation function from the oxygen atom in water to the CT2 carbon as described in section 2.1.

that the free energy of transfer of a CF_2 group from water to an air/water interface is more favorable than the transfer of a CH_2 group.[40] This suggests that CF_2 groups are more hydrophobic than CH_2 groups. The additional hydrophobicity of CF_2 groups could impact the stability of CO_2/water microemulsions by affecting the hydrophilic/CO_2-philic balance and the structure of water at the interface.

The additional penetration of water into the surfactant layer correlates with the structure of the surfactant. The phosphate headgroup would like to maximize hydrogen bonding between the oxygens in the headgroup and water. Increasing hydrogen bonding is more energetically favorable for the surfactant. The tails wish to point into the CO_2 phase because of favorable solvation of the tails by CO_2 and unfavorable solvation in the water phase. In the hydrocarbon, this is relatively easy because water penetrates somewhat into the surfactant. Thus, the headgroup has sufficient conformational freedom without sacrificing hydrogen bonding. For the fluorocarbon, however, this appears not to be the case. Since water penetration into the surfactant layer is reduced, hydrogen bonding to the phosphate oxygens would be sacrificed to point the tail into the CO_2 phase. Figure 6 depicts the net result of competitive hydrogen bonding. Tail 1 has sacrificed hydrogen bonding of its OS atom, while

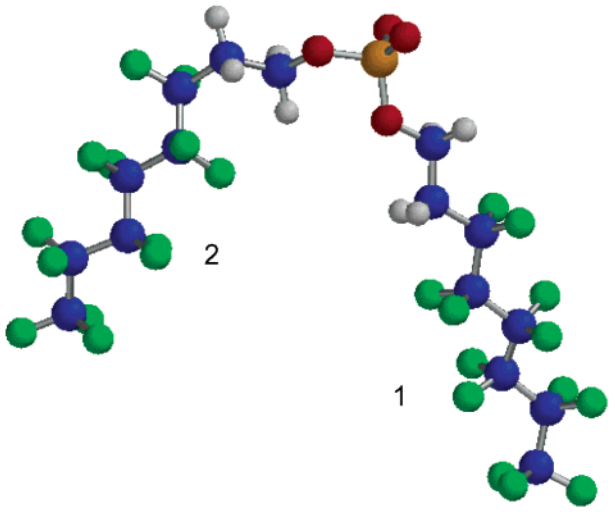

Figure 6. Visual representation of hydrogen bonding competition. This is a rendering of one of the surfactant molecules from system F116.

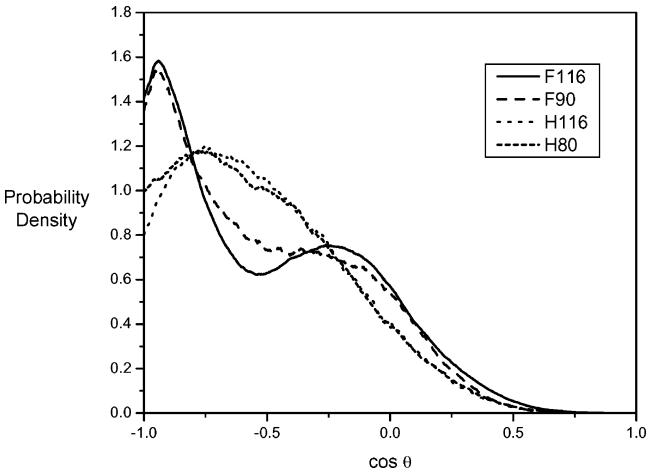

Figure 7. Distribution of the angle of the OS−P bond relative to the normal to the interface. A value of −1 indicates that the bond points directly into the CO_2 phase, whereas a value of 1 shows the bond pointing directly into the water phase.

tail 2 adopts a tilted conformation allowing hydrogen bonding between water and one OS atom.

The orientation of the headgroup can be described by the angle that the OS−P bond makes with the normal to the interface. If the cosine of the OS−P angle with the interface is near −1, then the OS atom is closer to the CO_2 phase. This OS atom sacrifices hydrogen bonding with water. If the cosine of the OS−P angle is closer to 0 (bond parallel to the interface), then the OS atom is exposed to the water phase. Figure 7 shows the distribution of the angle the OS−P bond makes with the interface. The difference between the fluorocarbons and hydrocarbons is rather striking. The fluorocarbons have a bimodal distribution of this angle. This order decays slightly at lower area, presumably due to steric constraints. The hydrocarbons have a single peak and do not show a marked preference to point an OS−P bond directly into the CO_2 phase. Figure 7 suggests that there are two distinct states for the OS−P bond in the chains of the surfactants. We classify the chains based on the angle the OS−P bond makes with the phosphorus plane. Chains whose OS−P bond has an angle whose cosine is less than −0.5 are classified as "perpendicular"; other chains are classified as "parallel". This value corresponds approximately to the minimum in the distribution for the fluorocarbon at the largest area, and it will be used to classify all the chains.

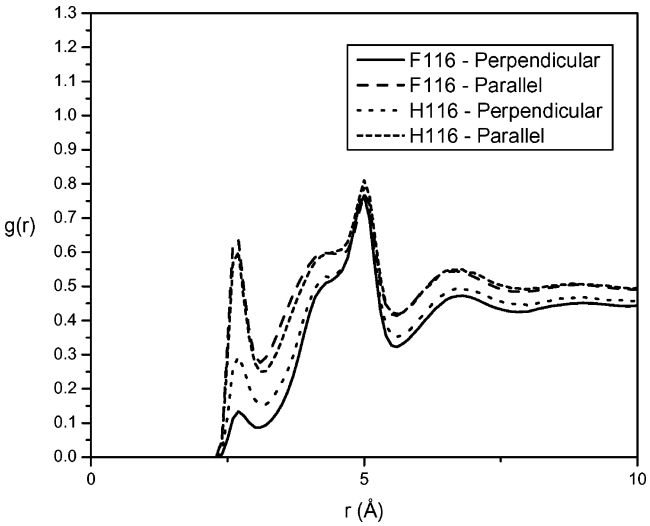

Figure 8. Pair correlation function from parallel and perpendicular OS atoms to oxygen atoms in water. Perpendicular OS atoms have a OS−P angle as described in Figure 7 whose cosine is less than −0.5. All other OS atoms are described as parallel.

The fluorocarbon surfactants must sacrifice hydrogen bonding with the OS oxygen atoms to align their tails away from water. Figure 8 shows evidence that hydrogen bonding is responsible for this phenomenon. The pair correlation function between OS and the water oxygen for parallel OS atoms, in both the hydrocarbon and the fluorocarbon, shows a distinct peak at 2.8 Å, which is approximately the nearest neighbor O−O distance in water.[41] Perpendicular OS atoms have almost no peak at 2.8 Å in the fluorocarbon surfactants. Perpendicular OS atoms in the hydrocarbon surfactants show a slight peak at 2.8 Å. The apparent preservation of some hydrogen bonding even for hydrocarbon tails in the perpendicular orientation supports the view that water penetrates the hydrocarbon surfactants more than the fluorocarbon surfactants.

The competition between hydrogen bonding and tail solvation occurs because the tails prevent water from penetrating the surfactant layer to a large extent. For the fluorocarbon surfactant, this manifests itself in one OS atom sacrificing nearly all hydrogen bonding and pointing directly into the CO_2 phase. The parallel OS atom lies nearly parallel to the interface, maintaining hydrogen bonding. For the hydrocarbon surfactant, there is less competition. The tails can be solvated with less concern about the hydrogen bonding penalty.

In addition to added penetration of water, hydrocarbon surfactants also manifest the penetration of CO_2 into the surfactant layer. These effects, when coupled, translate into additional CO_2/water contacts at the interface. CO_2/headgroup and water/tail contacts are also increased. These additional contacts are unfavorable, causing a higher surface tension, compared to that of an ideal interface. Additional penetration by CO_2 into the surfactant layer can be seen through an analysis of the density profiles from the average z-plane of the phosphorus atoms. For quantification, the density profiles are fit to the functional form[42]

$$\rho = \rho_{sol} + 0.5\rho_{bulk}\left(1 + \tanh\left(\frac{(z - z_0)}{w}\right)\right) \qquad (11)$$

ρ_{sol} accounts for the possibility that one phase is slightly soluble in the other, which is true for CO_2/water systems. ρ_{bulk} represents the bulk phase density far away from the interface. z_0 gives information about the position of the interface, and w shows the width of the interface.

TABLE 2: Results of Fitting the Density Profiles for Water and CO_2 to Eq 11[a]

simulation	CO_2		water		separation, $\lvert\Delta z_0\rvert$ (Å)	penetration parameter, P
	z_0 (Å)	w (Å)	z_0 (Å)	w (Å)		
F116	6.56	6.56	0.13	2.06	6.43 ± 0.07	1.34 ± 0.03
F90	8.73	5.28	−0.247	2.15	8.98 ± 0.09	0.83 ± 0.02
H116	4.99	5.8	0.29	2.23	4.7 ± 0.1	1.71 ± 0.07
H80	7.14	5.75	0.043	2.24	7.10 ± 0.07	1.13 ± 0.03

[a] See text for a definition of the penetration parameter and separation distance.

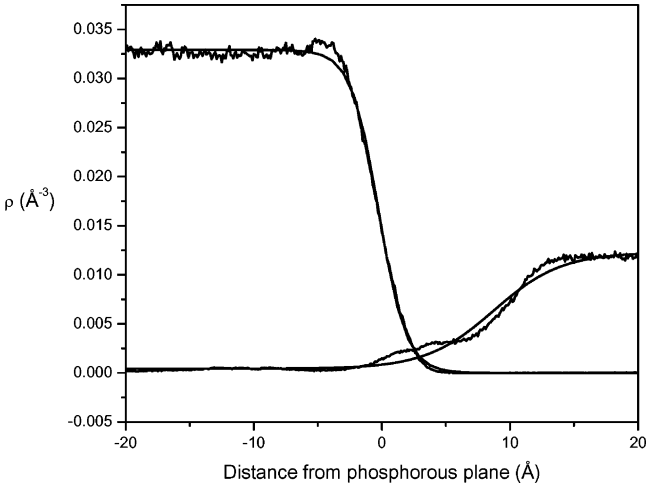

Figure 9. Density profiles for both water and CO_2 for system F90. The water profile has a maximum on the left side of the figure; the CO_2 profile has a maximum on the right. The data are the jagged lines with the fitted smooth lines close by.

The results of fitting the simulated density profiles to eq 11 are listed in Table 2. Figure 9 shows one of the fits. The separation distance in Table 2 is defined as the absolute value of the difference in the z_0 parameters. The surface tension is seen to correlate well with the separation distance between the two phases. A new interfacial parameter, termed here the penetration parameter (P), is defined as

$$P = \frac{w(\mathrm{CO_2}) + w(\mathrm{water})}{|z_0(\mathrm{CO_2}) - z_0(\mathrm{water})|} \tag{12}$$

This should indicate the degree to which the two phases come into contact in the interfacial region. Systems with broad distributions that are relatively close together will have more CO_2 and water density within the surfactant layer and a large value of the penetration parameter. Systems with relatively narrow distributions, separated by large distances compared to their widths, will separate the phases more effectively and will be characterized by small values of the penetration parameter. We note that the penetration parameter and the separation distance may be accessible experimentally by neutron reflectivity; density profiles such as eq 11 also can be fit to neutron data.

From Table 2, we see that the fluorocarbon is better able to separate the water and CO_2 phases from each other, as measured by the penetration parameter and the separation distance. Additional separation and less penetration correlate with low surface tension.

Correspondingly, evidence of greater penetration by CO_2 into hydrocarbon surfactants is provided by the pair correlation function of CO_2 to the CT2 carbon (see Figure 1), shown in Figure 10. The CO_2 density near the CT2 carbon correlates with the penetration parameter, shown in Table 2, and with the

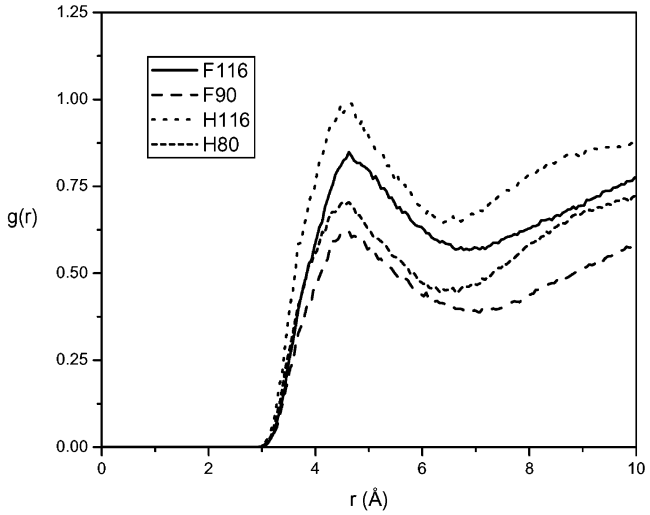

Figure 10. Pair correlation function from the carbon atom in CO_2 to the CT2 carbon (see Figure 1), the second carbon atom from the phosphorus atom, as described in section 2.1.

surface tension. At comparable areas, CO_2 has a much greater contact with the CT2 carbon of the hydrocarbon surfactants than that of the fluorocarbon surfactants. Yee et al. have measured changes in the vibrational modes of CO_2 in fluorocarbon solvents that they attribute to a depletion layer near CO_2,[43] consistent with the idea that enhanced solvation by CO_2 near the fluorocarbons is not a critical feature differentiating hydrocarbons and fluorocarbons.

The use of the phrase "CO_2-philic" to describe tails carries with it the connotation of enhanced solvent−tail energetic stabilization. The interaction energy should be affected by both the size of the tail and the density of CO_2 near the tail. Larger molecules tend to have stronger van der Waals attractive forces, due to both increased contact area and increased polarizability. Since the fluorocarbons are larger, they should have more favorable interactions with CO_2 on a contact area basis, although fluorine is well-known to carry a relatively low dispersion contribution due to its relatively low polarizability. In the present study, we see that the CO_2 density near the tails is larger for the hydrocarbon, as evidenced by the penetration parameter (Table 2), the pair correlation function between the CT2 carbon and CO_2 (Figure 10), and the density profiles for CO_2 (Figure 3). The simplest models for solvation show that the energy of interaction scales linearly with local density. This basis would suggest that hydrocarbons might have stronger interaction with CO_2. Further, the fluorocarbons have more charge separation due to the electronegativity of the fluorine atom, which has led some to consider a specific interaction between CO_2 and fluorocarbons.[8,21] A priori, it is difficult to estimate how these factors will balance.

From our simulations, we can calculate the interaction of CO_2 with the surfactant tails to answer this question, at least for the present model. The results of this calculation are listed in Table 3.

The energies are calculated from configurations taken at 1 ps intervals from the simulation. The Ewald summation is not used to calculate the Coulombic energies reported in Table 3; these energies give a valid basis for comparing the different systems, while allowing for facile separation of the CO_2/tail interactions from other components. The tail is defined as the portion of the surfactant past and including the CT2 carbon group, that is, carbons CT2 through CT8 on the hydrocarbons and CT2 through CF6 for the fluorocarbons. The CT1 methylene

TABLE 3: Normalized Average Energy of Interaction between a Surfactant Tail and CO_2, Broken down by Contribution[a]

system	total energy	van der Waals energy	Coulombic energy
F116	−21.0	−20.55	−0.45
F90	−17.2	−16.8	−0.37
H116	−20.8	−20.8	−0.01
H80	−16.4	−16.4	−0.01

[a] The energies reported only include CO_2/tail interactions; no tail/tail or tail/water interactions are included. All energies are reported as E/kT. Errors in the energies are $0.3kT$.

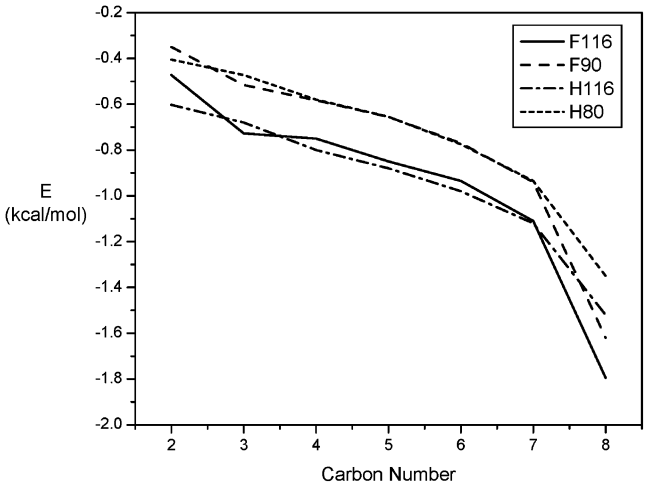

Figure 11. Energy of carbon groups (CH_2, CF_2, CF_3, or CH_3) with CO_2. The carbon number refers to number of carbon atoms from the phosphorus atom; that is, carbon CT2 is carbon 2, CT3 and CF1 are carbon 3, and so forth.

group has a net charge due to the carbon−oxygen bond, and hence, it is not included as part of the defined tail.

The net Coulombic portion of the interaction between CO_2 and fluorocarbons is very weak, for the OPLS model. This energy only accounts for an additional $0.4kT$ of favorable interaction. This offers evidence that little specific interaction exists between CO_2 and fluorocarbons. In the OPLS model, such specific interactions would necessarily be Coulombic in nature. Other researchers have also seen little evidence for specific interactions between CO_2 and fluorocarbons.[43−46] In our simulations, the primary competition is between somewhat more favorable van der Waals interaction parameters for the fluorocarbons and greater local CO_2 density for the hydrocarbons. The local CO_2 density does have a significant effect on the energy, as can be seen by comparing systems with the same surfactant at different areas. Smaller areas allow less penetration into the surfactant layer (Table 2). The drop in CO_2 density caused by lowering the area per molecule from 116 to 90 Å^2 for the fluorocarbon surfactant resulted in the loss of approximately $3.8kT$ of favorable interactions.

The energy of interaction can also be calculated on a per group basis, that is, CH_2, CF_2, CF_3, or CH_3. Figure 11 shows the energy broken down by group. The main difference in the energy of interaction of the fluorocarbons and hydrocarbons is in the terminal CF_3 group compared to the CH_3 group. This is expected because the penetration of CO_2 into the surfactant layer likely has less influence on the interactions of the end group. End groups tend to stay at the boundary of the surfactant layer (Figure 2), where the CO_2 density is near its bulk value (Figure 3). On the interior of the surfactants, the differences between fluorocarbon and hydrocarbon interactions are more subtle. The

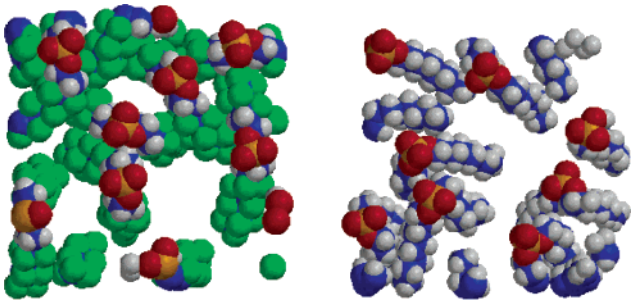

Figure 12. Top down view of one interface after 500 ps of simulation time. The left picture is simulation F116; the right picture is simulation H116. The fluorocarbon surfactant clearly occupies more space at the interface separating the CO_2 and water.

CO_2 penetration and larger size appear to be nearly perfectly balanced in this region for the present case. Finally, we note that the interfacial tension and the interaction energy between CO_2 and the tails do not correlate very well.

All of these simulation results strongly suggest that the feature that distinguishes hydrocarbon from fluorocarbon surfactants is their relative ability to prevent water and CO_2 from penetrating the surfactant layer. While the interactions of the tail with CO_2 are important, they do not distinguish these cases. The tail must force water and CO_2 to separate. Our results indicate that a fluorocarbon tail correlates with less CO_2 penetration into the surfactant layer. One mechanism for this is the large size of the fluorine atom relative to a hydrogen atom forcing CO_2 and water away from the interface via simple excluded volume. This results in fewer CO_2/water contacts at the interfacial region. CO_2/headgroup and water/tail contacts are also reduced. Since CO_2/water contacts are relatively unfavorable, as evidenced by the surface tension, these contacts result in a free energy penalty. Our evidence suggests that hydrocarbons do not make as good surfactants because, in general, they are too small, not because they cannot be solvated by CO_2. This can be seen visually in Figure 12. The fluorocarbon clearly occupies more space at the interface. Hydrocarbon surfactants are also relatively less hydrophobic, allowing relatively greater penetration of water, as reflected in the penetration parameter.

4. Conclusion

We have studied the analogous surfactants DiF8 and DiH8 under conditions of comparable area per surfactant. Earlier work would suggest that such conditions are appropriate.

The present work has led to specific conclusions about the behavior of DiF8 and DiH8. First, water penetrates the hydrocarbon surfactant more than the fluorocarbon surfactant. The coordination number of the OS atoms in the surfactant shows that water solvates the hydrocarbon OS atoms better. Also, the pair correlation function from the CT2 carbon to water shows that water reaches this particular carbon more frequently in hydrocarbon surfactants than in fluorocarbon surfactants.

This headgroup hydration pattern occurs despite structural accommodation in the fluorocarbon case. The unusual orientation of the headgroup at the CO_2/water interface for the fluorocarbon surfactant results from favorable headgroup hydrogen bonding competing with the tail's preference to reside in the CO_2 phase. For the hydrocarbon surfactant, there is less competition because water penetrates to the OS atom and allows favorable hydrogen bonding. In the fluorocarbons, the OS atom must tilt the headgroup to gain favorable hydrogen bonding interactions. This sacrifices the other OS atom directly into the CO_2 phase.

CO_2 is also found to penetrate the hydrocarbon surfactant to a greater extent than the fluorocarbon surfactant at comparable areas. The pair correlation function between carbon dioxide and the CT2 carbon atom shows that CO_2 has more contact with the CT2 atom in the hydrocarbon surfactant than in the fluorocarbon surfactant. An analysis of the density profile of CO_2 also shows greater CO_2 penetration in the hydrocarbon surfactants. This suggests that good tail solvation, while important, can hamper surfactant quality by allowing too much contact between components of the bulk solvent, increasing the surface tension. We infer that hydrocarbon surfactants fail because they allow both water and CO_2 to penetrate the surfactant layer, resulting in a high surface tension. This is evidently primarily a result of the small size of hydrocarbon tails.

A new surfactant parameter has been developed and calculated to quantify the "contact", named the penetration parameter, *P*. *P* gives an experimentally accessible measurement of how well the surfactant minimizes contacts between the two bulk phases. These calculated values are found to correlate with the surface tensions for DiF8 and DiH8.

Future design of surfactants should attempt to minimize penetration. "Stubby" surfactants are a promising means to realize this goal. Adding methyl groups to the hydrocarbon tails aids surfactant quality.[20,47,48] This has been attributed to a better cohesive energy density match between CO_2 and methyl groups.[20] However, the present work suggests that the bulkier chains are better able to exclude CO_2 and water from the surfactant layer, resulting in lower surface tensions. Additional theoretical and experimental work is underway to establish the validity of this novel conclusion.

Acknowledgment. We would like to thank the Texas Advanced Computing Center for computational support. This material is based upon work supported in part by the STC Program of the National Science Foundation under Agreement No. CHE-9876674 and by the R. A. Welch Foundation. We are grateful to Max Berkowitz and Sanjib Senapati for help in the development of the molecular dynamics algorithms used.

Supporting Information Available: Tables of surfactant potential parameters, charge distributions of surfactant, bond stretching parameters, bond angle parameters, and dihedral potentials and a figure showing sample FIELD and CONTROL files for DL_POLY. This material is available free of charge via the Internet at http://pubs.acs.org.

References and Notes

(1) Johnston, K. P.; Harrison, K. L.; Clarke, M. J.; Howdle, S. M.; Heitz, M. P.; Bright, F. V.; Carlier, C.; Randolph, T. W. *Science* **1996**, *271*, 624.

(2) Kane, M. A.; Baker, G. A.; Pandey, S.; Bright, F. V. *Langmuir* **2000**, *16*, 4901.

(3) Jacobson, G. B.; Lee, C. T., Jr.; da Rocha, S. R. P.; Johnston, K. P. *J. Org. Chem.* **1999**, *64*, 1207.

(4) Shah, P. S.; Holmes, J. D.; Doty, R. C.; Johnston, K. P.; Korgel, B. A. *J. Am. Chem. Soc.* **2000**, *122*, 4245.

(5) DeSimone, J. M. *Science* **2002**, *297*, 799.

(6) Lee, C. T., Jr.; Bhargava, P.; Johnston, K. P. *J. Phys. Chem. B* **2000**, *104*, 4448.

(7) Lee, C. T., Jr.; Johnston, K. P.; Dai, H. J.; Cochran, H. D.; Melinchenko, Y. B.; Wignall, G. D. *J. Phys. Chem. B* **2001**, *105*, 3540.

(8) Hoefling, T. A.; Enick, R. M.; Beckman, E. J. *J. Phys. Chem.* **1991**, *95*, 7127.

(9) Harrison, K.; Goveas, J.; Johnston, K. P. *Langmuir* **1994**, *10*, 3536.

(10) Eastoe, J.; Cazelles, B. M. H.; Steytler, D. C.; Holmes, J. D.; Pitt, A. R.; Wear, T. J.; Heenan, R. K. *Langmuir* **1997**, *13*, 6980.

(11) Downer, A.; Eastoe, J.; Pitt, A. R.; Simister, E. A.; Penfold, J. *Langmuir* **1999**, *15*, 7591.

(12) Eastoe, J.; Downer, A.; Paul, A.; Steytler, D. C.; Rumsey, E.; Penfold, J.; Heenan, R. K. *Phys. Chem. Chem. Phys.* **2000**, *2*, 5235.

(13) Liu, Z.-T.; Erkey, C. *Langmuir* **2001**, *17*, 274.

(14) Eastoe, J.; Paul, A.; Downer, A.; Steyler, D. C.; Rumsey, E. *Langmuir* **2002**, *18*, 3014.

(15) Sagisaka, M.; Yoda, S.; Takebayashi, Y.; Otake, K.; Kitiyanan, B.; Kondo, Y.; Yoshino, N.; Takebayashi, K.; Sakai, H.; Abe, M. *Langmuir* **2003**, *19*, 220.

(16) Keiper, J. S.; Simhan, R.; DeSimone, J. M. *J. Am. Chem. Soc.* **2002**, *124*, 1834.

(17) Steytler, D. C.; Rumsey, E.; Thorpe, M.; Eastoe, J.; Paul, A.; Heenan, R. K. *Langmuir* **2001**, *17*, 7948.

(18) Liu, J.; Han, B.; Li, G.; Zhang, X.; He, J.; Liu, Z. *Langmuir* **2001**, *17*, 8040.

(19) Liu, J.; Hand, B.; Wang, Z.; Zhang, J.; Li, G.; Yang, G. *Langmuir* **2002**, *18*, 3086.

(20) Ryoo, W.; Webber, S. E.; Johnston, K. P. Water-in-carbon dioxide microemulsions with methylated branched hydrocarbon surfactants. Submitted.

(21) Sarbu, T.; Styranec, T.; Beckman, E. J. *Nature* **2000**, *405*, 165.

(22) da Rocha, S. R. P.; Harrison, K. L.; Johnston, K. P. *Langmuir* **1999**, *15*, 419.

(23) Gelbart, W. M.; Ben-Shaul, A. *J. Phys. Chem.* **1996**, *100*, 13169.

(24) da Rocha, S. R. P.; Johnston, K. P.; Westacott, R. E.; Rossky, P. J. *J. Phys. Chem. B* **2001**, *105*, 12092.

(25) da Rocha, S. R. P.; Johnston, K. P.; Rossky, P. J. *J. Phys. Chem. B* **2002**, *106*, 13250.

(26) Schurhammer, R.; Berny, F.; Wipff, G. *Phys. Chem. Chem. Phys.* **2001**, *3*, 647.

(27) Schurhammer, R.; Wipff, G. *New J. Chem.* **2002**, *26*, 229.

(28) Baaden, M.; Schurhammer, R.; Wipff, G. *J. Phys. Chem. B* **2002**, *106*, 434.

(29) Salaniwal, S.; Cui, S. T.; Cochran, H. D.; Cummings, P. T. *Langmuir* **2001**, *17*, 1773.

(30) Salaniwal, S.; Cui, S. T.; Cochran, H. D.; Cummings, P. T. *Langmuir* **2001**, *17*, 1784.

(31) Senapati, S.; Keiper, J. S.; DeSimone, J. M.; Wignall, G. D.; Melinchenko, Y. B.; Frielinghaus, H.; Berkowitz, M. L. *Langmuir* **2002**, *18*, 7371.

(32) Harris, J. G.; Yung, K. H. *J. Phys. Chem.* **1995**, *99*, 12021.

(33) Berendsen, H. J. C.; Grigera, J. R.; Straatsma, T. P. *J. Phys. Chem.* **1987**, *91*, 6269.

(34) Chun, B.-S.; Wilkinson, G. T. *Ind. Eng. Chem. Res.* **1995**, *34*, 4371.

(35) Jorgensen, W. Personal communication, 2002.

(36) Smith, W.; Forester, T. R. *DL_POLY Package for Molecular Dynamics Simulations*, 2.12 ed.; Daresbury Laboratory: Daresbury, Warrington, England, 1999.

(37) Parrinello, M.; Rahman, A. *J. Appl. Phys.* **1981**, *52*, 7182.

(38) Zhang, Y.; Feller, S. E.; Brooks, B. R.; Pastor, R. W. *J. Chem. Phys.* **1995**, *103*, 10252.

(39) da Rocha, S. R. P.; Johnston, K. P. *Langmuir* **2000**, *16*, 3690.

(40) Mukerjee, P.; Handa, T. *J. Phys. Chem.* **1981**, *85*, 2298.

(41) Narten, A. H.; Levy, H. A. *J. Chem. Phys.* **1971**, *55*, 2263.

(42) Lu, J. R.; Hromadova, M.; Thomas, R. K.; Penfold, J. *Langmuir* **1993**, *9*, 2417.

(43) Yee, G. G.; Fulton, J. L.; Smith, R. D. *J. Phys. Chem.* **1992**, *96*, 6172.

(44) Diep, P.; Jordan, K. D.; Johnson, J. K.; Beckman, E. J. *J. Phys. Chem. A* **1998**, *102*, 2231.

(45) Yonker, C. R. *J. Phys. Chem. A* **2000**, *104*, 685.

(46) Raveendran, P.; Wallen, S. L. *J. Phys. Chem. B* **2003**, *107*, 1473.

(47) Eastoe, J.; Paul, A.; Nave, S.; Steytler, D. C.; Robinson, B. H.; Rumsey, E.; Thorpe, M.; Heenan, R. K. *J. Am. Chem. Soc.* **2001**, *123*, 988.

(48) da Rocha, S. R. P.; Dickson, J.; Cho, D.; Rossky, P. J.; Johnston, K. P. *Langmuir* **2003**, *19*, 3114.